**Paper:**

Zhang, L., Belblidia, F., Davies, H., Lavery, N. & Brown, S. Optimizing gate location to reduce metal wastage: Co-Cr-W alloy filling simulation. *Journal of Materials Processing Technology*

# Accepted Manuscript


Title: Optimizing gate location to reduce metal wastage: Co-Cr-W alloy filling simulation

Author: Lintao Zhang Fawzi Belblidia Helen M. Davies Nicholas P. Lavery Stephen G.R. Brown Dyfyr Davies

PII: S0924-0136(16)30352-1
DOI: http://dx.doi.org/doi:10.1016/j.jmatprotec.2016.09.027
Reference: PROTEC 14979

To appear in: *Journal of Materials Processing Technology*

Received date: 16-6-2016
Revised date: 27-9-2016
Accepted date: 30-9-2016

Please cite this article as: Lintao Zhang, Fawzi Belblidia, Helen M. Davies, Nicholas P. Lavery, Stephen G.R. Brown, Dyfyr Davies, Optimizing gate location to reduce metal wastage: Co-Cr-W alloy filling simulation, *<![CDATA[Journal of Materials Processing Tech.]]>* (2016), http://dx.doi.org/10.1016/j.jmatprotec.2016.09.027

# Optimizing gate location to reduce metal wastage: Co-Cr-W alloy filling simulation

Lintao Zhang[a,*], Fawzi Belblidia[a], Helen M. Davies[a], Nicholas P. Lavery[a], Stephen G.R. Brown[a], Dyfyr Davies[b]

[a] *Advanced Sustainable Manufacturing Technologies (ASTUTE2020) Operation, College of Engineering, Swansea University, Bay Campus, Fabian Way, Swansea SA1 8EN, UK*
[b] *Weartech International Ltd., Moor Road,Baglan Industrial Estate, Port Talbot SA12 7BJ, UK*

**Abstract**

This research aimed at reveal the reasons for the extra Co-Cr-W alloy wastage in the risers in sand casting. The alloy filling behaviour in both the original and modified moulds was investigated numerically. The alloy-air interface was captured by using Volume of Fraction method. For the original mould, an unfilled volume in the vicinity of the runner bar top was apparent and it was refilled by a back flow, originated from the risers in the late stage of filling. The back flow behaviour required a higher level of the liquid alloy in the risers, which resulted in excessive wastage, and it was essential to form the required shape of the cast. For the modified mould, the unfilled volume was eliminated and the cast part shaping time was reduced to around 10 s from 90 s. The alloy wastage in the risers was reduced by 11%.

*Keywords:* Sand casting, Mould design, Co-Cr-W alloy, Computational fluid dynamics, Filling behaviour

## 1. Introduction

Sand casting process involves two main stages: the filling stage and the solidification stage. Investigations on the filling stage are critical with regards

*Corresponding author
*URL:* L.Zhang@swansea.ac.uk (Lintao Zhang)

to several aspects, for example, the configuration optimization and the metal wastage analysis.

For the filling stage, the simulation can give a visualization of the filling of the mould. This cannot be observed in the experiment due to closed sand mould. Therefore, the numerical simulation is a powerful tool compared to the experimental research. Several numerical schemes were introduced to capture the movement of interface between the air and the liquid alloy in the filling stage. The VOF-Leer scheme was adopted to simulate the three-dimensional filling behaviour of the liquid metals in the mould through two cases (Chan et.al., 1991): slow filling to the large scale sand-casting mould and a die-casting process. This technique provided the realistic results that were validated by experiments. For a transient simulation, the pesudo-concentration formulation was also adopted (Ravindran and Lewis, 1998) to track the movement of the metal front on a fixed mesh. This selection avoided the difficulties that usually occurred when a step function was transported by the pure advection. An adaptive grid method was developed for the tetrahedral and hexahedral elements to simulate the mould filling for casting process Kim (Kim et.al., 2006). A sharp interface solution algorithm (SOLA) particle level set method based on the finite difference analysis was considered by Pang (Pang et.al., 2010). This straightforward method was successfully validated against the benchmark simulation (Sirrell et.al., 1995). To take into account the effect of the sand mould coating permeability, a mathematical model was developed based on the SOLA-Volume Of Fraction (SOLA-VOF) technique (Mirbagheri et.al., 2003) and the results were validated by the experiment of aluminium alloy within a transparent mould. By coupling the new model and 3D-VOF techniques, the error for mould filling time was reduced to 16%. More importantly, the investigation of the liquid metal filling behaviour were also used to optimize the sand mould configurations, e.g. the gating systems (Kermanpur et.al., 2008; Sun et.al., 2008; Du et.al., 2015). Experimentally, Assar (Assar, 1999) showed the influence of the filling mass flow rate on the microstructure of Al-4.5Cu ingots, especially that the coarser equiaxed grains and short columnar grains were obtained as the filling rate was increased. The filling direction (top and botttom) also had the effect on the tensile strength of the air cast 2L99 Al-Si-Mg alloy, 254-SMO super duplex stainless steel and vacuum cast IN939 nickel based superalloys, respectively (Cox et.al., 2000).

The present research is based on an industrial problem, raised by a local company. The main concerns of the company can be summarized as follows:

1. the filling behaviour of Co-Cr-W alloy in a specified (original) mould configuration,
2. the solutions to reduce the extra alloy wastage in both risers, which was categorised as "revert".

To address the above two concerns, the characterization of the liquid Co-Cr-W alloy filling behaviour within the specific mould configuration shall be conducted. The ultimate aim is to optimize the mould design to reduce the extra alloy wastage in risers. The outline of the present paper is as follows. The configuration and the numerical system are introduced in section 2. In section 3.1, the filling dynamics, in the region prior to the runner bar gate are assessed. In section 3.2, the flow behaviour beyond the runner bar gate is analysed, and finally the filling process for the modified mould configuration is discussed in section 3.3. Main conclusions are summarized in section 4.

## 2. Configuration and numerical system

### *2.1. Configuration*

Fig.1 showed the cast sample which was originated from the sand mould. The various parts of the mould were labelled in Fig.1. The cast sample reflects the inner configuration of the sand mould. The diameter of the runner bar (Label 7 in Fig.1) is 35 mm. The company noticed that for this particular mould configuration, a certain height of alloy in the risers (Label 6 and 8 in Fig.1) is essential to ensure to shape the cast. However, this certain height of the alloy results in the extra alloy wastage ("revert"), as shown in Fig.1.

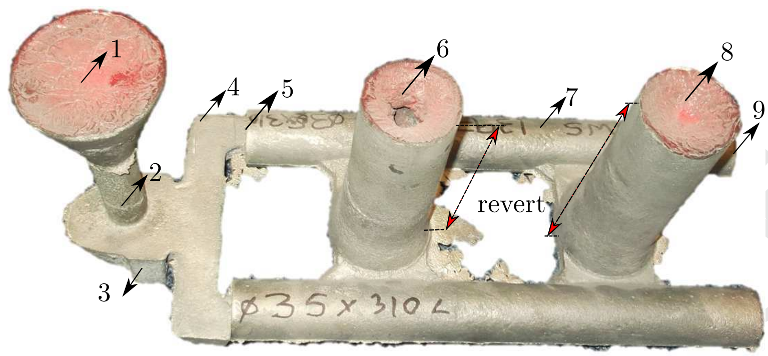


Figure 1: Cobalt-Chrome-Tungsten alloy cast. Different parts of the cast are named as the pouring basin (1), the sprue (2), the choke (3), the turning part region (4), the runner bar inlet (5), the front riser (6), the runner bar (7), the rear riser (8) and the runner bar end wall (9), respectively.

### *2.2. Governing equations and numerical system*

The filling behaviour of liquid Co-Cr-W alloy (density $\rho$, 8300 kg$\cdot$ m$^{-3}$, dynamic viscosity $\mu$, 0.004 kg $\cdot$m $^{-1}\cdot$s$^{-1}$(Carswell et.al., 2011)) in a sand mould was investigated, by using Volume of Fluid (VoF) model based on the finite volume technique available in ANSYS® FLUENT (version: 15.0). The liquid alloy flow behaviour is governed by the incompressible flow Navier-Stokes equations:

$$\partial_t \rho + \nabla \cdot \mathbf{u} = 0, \tag{1}$$

$$\partial_t \mathbf{u} + (\mathbf{u} \cdot \nabla)\mathbf{u} + \frac{\nabla p}{\rho} = \nu \nabla^2 \mathbf{u} + \frac{1}{\rho}\mathbf{F}_g, \tag{2}$$

where $\mathbf{u}$, $\nabla p$, $\nu$ and $\mathbf{F}_g$ are velocity, pressure gradient, kinematic viscosity and the gravity force, respectively. VoF model was adopted as the multiphase model to capture the interface between the liquid alloy phase ($L$-phase) and the air phase ($A$-phase). The VoF method, which has been well validated (Sun et.al., 2012; Hargreaves et.al., 2014), is based on pressure-based solver, and allows to simulate two or more immiscible fluids by tracking the volume fraction of each fluid in the whole computing domain (ANSYS, Inc., 2013). In the VoF model, the interface between $L$-phase and $A$-phase is captured by solving the Eq.(1) for the volume fraction of different phases. For $L$-phase, Eq.(1) can be rewritten as:

$$\partial_t(\alpha_L \rho_L) + \nabla \cdot (\alpha_L \rho_L \mathbf{u}_L) = S_L + \sum_{n=1}^{2} (\dot{m}_{AL} - \dot{m}_{LA}), \tag{3}$$

where $\dot{m}_{AL}$ (resp. $\dot{m}_{LA}$) denotes the mass transfer from $L$ (resp. $A$) phase to $A$ (resp. $L$) phase. $\alpha_L$ denotes the volume of fraction of phase $L$ in the cell. Therefore, for a single cell:

$$\alpha_L = \begin{cases} 0 & \textit{empty of L-phase}, \\ 0 \leq \alpha_L \leq 1 & \textit{mixture of L-phase and A-phase}, \\ 1 & \textit{full of L-phase}. \end{cases} \tag{4}$$

In Eq.(3), $S_L$ is the source term of $L$-phase. In the present research, the continuity equation was shared by $L$-phase and $A$-phase. The mass transfer between different phases was neglected and no source term was considered. Eq.(3) can be simplified as:

$$\partial_t(\alpha_L \rho_L) + \nabla \cdot (\alpha_L \rho_L \mathbf{u}_L) = 0. \tag{5}$$

For the $A$-phase, the volume of fraction can be obtained by the following constrain:

$$\alpha_L + \alpha_A = 1. \tag{6}$$

The filling process is much shorter than the solidification process so that an assumption could be considered: the flow behaviour is temperature independent (isothermal) during the filling stage. The SIMPLE scheme (Ferziger and Peric, 2002) was used to carry out the pressure-velocity coupling: a pressure was first assumed and then the velocity field was calculated by solving the Eq.(2). The determined velocity was put in the Eq.(5), until the continuity conservation was achieved by modifying the pressure. For the spatial and the time discretization schemes the second order upwind and the second order implicit scheme were adopted.

Due to the symmetric feature of the sand mould, only half of the geometry was considered. The coordinate system was defined as follows: -$z$ axis and $x$ axis were defined along the mainstream directions of the liquid alloy in the sprue and the runner bar, respectively. The sketch of the simulation domain

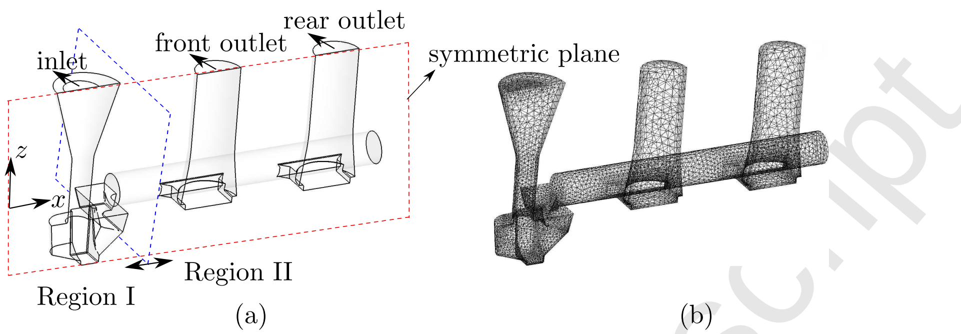


Figure 2: The simulation domain (a) and the mesh (b).

is shown in Fig.2(a). Region I and II refer to the regions before and after the runner bar gate. A user defined function of the mass flow rate $\dot{m}$, which normal to the inlet, was applied as the inlet boundary condition (Dirichlet boundary condition). The expression of $\dot{m}$ with simulation time $t_s$ is shown as following:

$$\dot{m} = \begin{cases} 0.5 & 0 \leq t_s \leq 10, \\ 0 & otherwise. \end{cases} \tag{7}$$

$\dot{m}$ and $t_s$ are in the unit of kg·s$^{-1}$ and s, respectively. The expression of $\dot{m}$ is considered a continuous flow feeding the inlet for 10 s and then the pouring behaviour is stopped to allow for the flow to settle down. For the front outlet and the rear outlet, the outflow boundary condition was adopted, with the flow rate weighting 0.5 and 0.5, respectively. The symmetric boundary condition was applied on the symmetric plane. The mesh sensitivity test was carried out to make sure the simulation results were mesh independent and ensured a good precision at a reasonable computing cost. The inflation layers were set in the vicinity of the boundaries with transition ration, maximum layer and growth rate were 0.272, 5 and 1.2, respectively, to capture the fluid behaviour near the walls. The unstructured mesh was used, as shown in Fig.2(b). The total number of the elements was 142742.

## 3. Results and discussion

Due to the complexity of the mould configuration, the cavity is presented by using two regions: Region I and Region II. The filling behaviour in Region I and II was discussed in section 3.1 and 3.2, respectively.

### *3.1. Filling behaviour in Region I*

#### *3.1.1. General features*

Fig.3 showed the snapshots of the interface variation between the liquid alloy phase and the air phase with $t_s$ in Region I: $\alpha_L$=0.5 (in green) for iso-surface and at $\alpha_L > 0.5$ (in grey) for iso-volume. The filling starts whilst the liquid

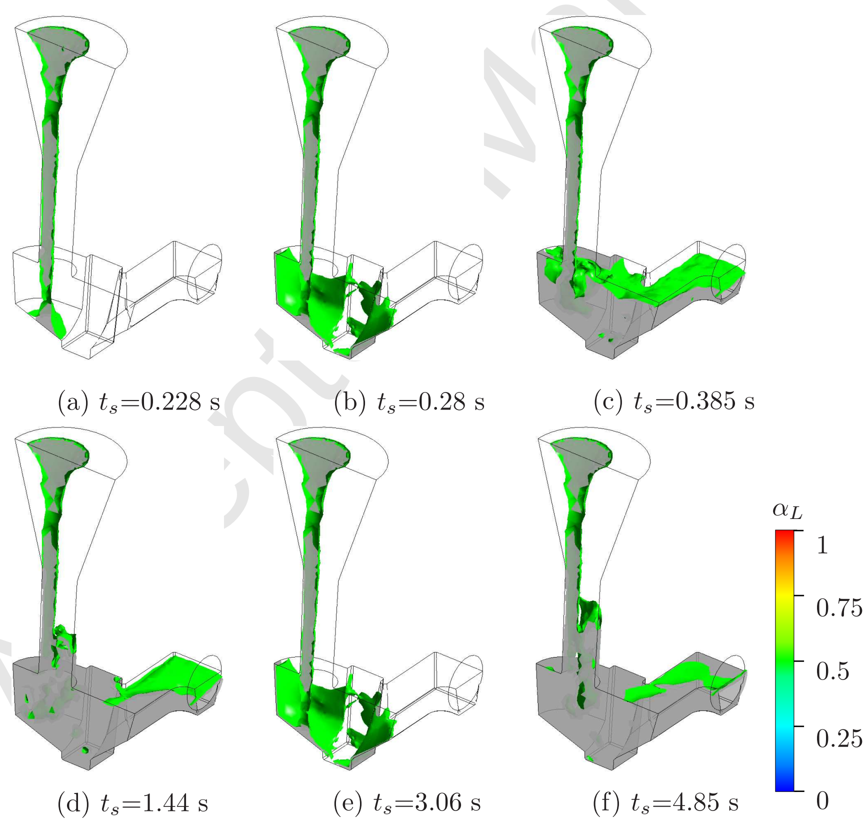


Figure 3: Snapshots of iso-surface of $\alpha_L$=0.5 (in green) and iso-volume of $\alpha_L > 0.5$ (in grey) in Region I at different $t_s$.

alloy enters the mould from the pouring basin. The flow, driven by the gravity (along -$z$ axis), reaches bottom of the choke through the sprue(Fig.3(a)). The existence of a half nodal-point (Hunt et.al., 1978) for the bottom of the choke wall is observed. The flow then spreads all the directions, whilst it remains attached to the choke bottom wall. In the choke region, the flow in the -$x$ direction forms a recirculation zone, which will be discussed in detail in the section 3.1.2. After the flow reaches the choke side wall, the flow level increases along $z$-axis direction until it reaches the choke top wall(Fig.3(b))). However, due to the gravity, the liquid alloy flows back to the bottom part(Fig.3(c)). The back flow movement generates the liquid recirculation and the height of which increases as the filling advances. Once the liquid level reaches the top wall of the choke region, the interactions between the recirculation flow and the main stream becomes dominant(Fig.3(d) and (e)). Under this condition, part of the flow flows back to the sprue zone, as shown in(Fig.3(f)).

Back to Fig.3(b), for the flow along $x$ direction, as the mainstream flow towards the runner bar region advances, the flow first meets the step for this particular geometry. This generates an anti-clockwise flow recirculation near the step region. At the turning part of the feeder region, the dynamics of flow is similar with the flow past and $90^o$ and $180^o$ sharp bend (Zhang and Pothèrat, 2013). The existence of the recirculation is observed near the corner region due to the adverse pressure gradient. After the flow passes through the feeder, the bottom and the turning part of Region I, it reaches Region II.

### *3.1.2. Flow in the choke*

Fig.4 showed the snapshots of the surface streamline ($x - z$ plane at $y =$ 0.001m, which is very close to the symmetric plane) and the $\alpha_L > 0.5$ (in grey) for iso-volume distribution with $t_s$. At the early stage of the filling, an air recirculation, $R^A$, is formed by the shear layer effect which is caused by the incoming flow, as shown in Fig.4 (a). The intensity of the $R^A$ increases with time $t_s$. Once the flow flows back under the gravity to the bottom wall of the choke, as discussed in the section 3.1.1, a liquid alloy recirculating region $R^L$ is generated, as shown in (b) and the height of the recirculation region is increased

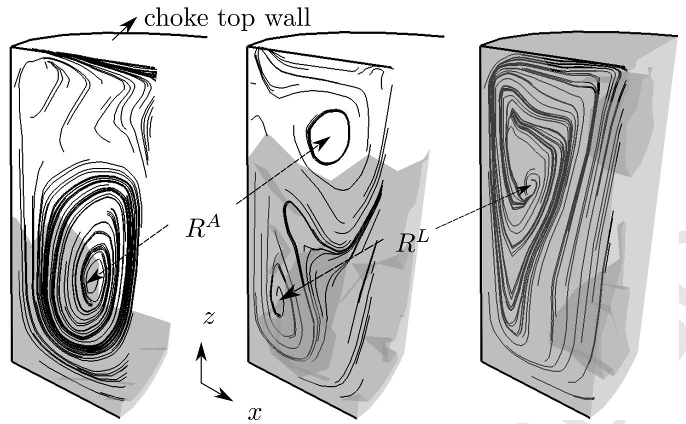


(a) $t_s$=0.25 s (b) $t_s$=0.78 s (c) $t_s$=2.01 s

Figure 4: Snapshots of iso-volume of $\alpha_l > 0.5$ (in grey) and surface streamline (in black) at $x - z$ plane when $y$=0.001 m at different $t_s$.

as the $t_s$ increases, whilst the recirculation R$^A$ slowly vanishes with rising level of the liquid alloy. As $t_s$ advances, e.g. $t_s$ = 2.01s, as shown in Fig.4 (c), the liquid alloy free level reaches the top wall of the choke, R$^L$ reaches the maximum size and R$^A$ vortex disappears.

### *3.2. Filling behaviour in Region II*

#### *3.2.1. General features*

Fig.5 showed the snapshots of the interface variation between the liquid alloy phase and the air phase with $t_s$ in Region II: $\alpha_L$=0.5 (in green) for iso-surface and at $\alpha_L > 0.5$ (in grey) for iso-volume. The mainstream of the liquid alloy first flows towards the runner bar end wall, as shown in Fig.5 (a). Due the effect of the runner bar end wall, a back flow with an opposite direction to the mainstream is generated. The liquid alloy level in the runner bar region increases as $t_s$ increases. The flow first enters the rear riser and then the front riser Fig.5(b) and (c), respectively. As the filling process advances, the liquid level in the riser increases. However, for the present configuration, the simulation has unveiled an unfilled region in the runner bar, Fig.5(d), whist the flow has already entered the risers. Interestingly, after the feeding is stopped ($t_s$ >10 s),

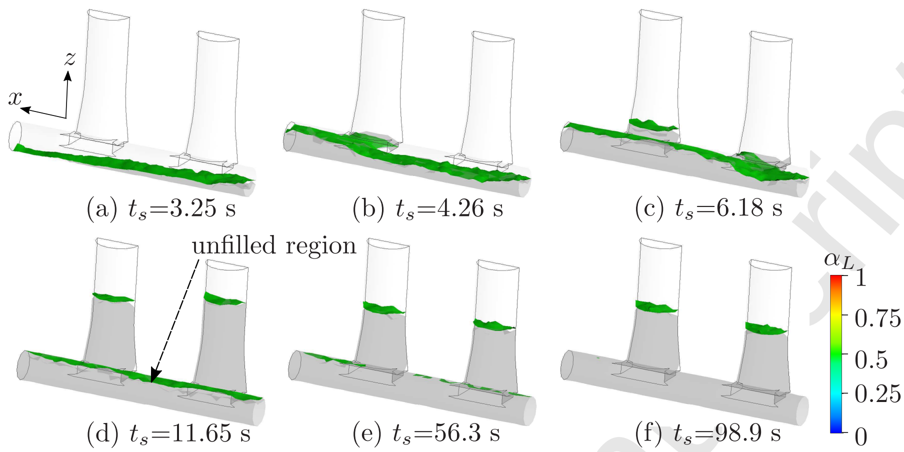


Figure 5: Snapshots of iso-surface of $\alpha_l$=0.5 (in green) and iso-volume of $\alpha_l$ > 0.5 (in grey) of Region II at different $t_s$.

there is a clear indication of the back-flow from both rear and front risers to the runner bar region to refill the unfilled volume Fig.5(e). The filling process is finally completed, as shown in Fig.5(f) with no existence of the unfilled region. The results indicate that the shaping time for the cast (runner bar region) is around 100 s. The total shaping time is nearly 10 times compared to the filling time (100 s *v.s.* 10 s). Furthermore, the splash behaviour, e.g. back flow originated from the risers, could further lead to the oxide films (Jolly, 2005; Campbell, 2004) and this behaviour should be avoided. Therefore, it will be critical important to reveal the flow behaviour in the final stage of the filling process, as the fluid dynamics can influence the microstructure of the casting in the region of runner bar and the risers.

### *3.2.2. Back flow refilling behaviour*

The back flow refilling process of the unfilled volume in the runner bar (Fig.5 (e)), identified by the simulation, can not be observed in the filling experiment. This is because that the mould cavity is entirely covered by the sand. This refilling behaviour is driven by a back flow which originates from the risers due to the gravity effect at the final stage of the filling process ($t_s$ >10 s). To capture this phenomenon and understand the flow dynamics, two cross-sections in the vicinity of inlets of front and rear risers ($x-z$ plane at $y=0.035$m) are selected, respectively. The velocity vectors were plotted on the cross-sections at $t_s$=9.95 s and $t_s$=10.36 s, as shown in Fig.6. The reason for

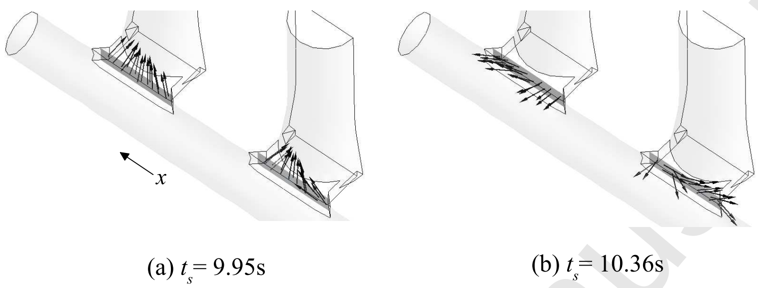


Figure 6: Distribution of the velocity vectors (normalized) at the surface near the inlets of the risers ($x-z$ plane, $y$=0.035m) at different $t_s$.

the selection of $t_s$=9.95 s and $t_s$=10.36 s is due to the inlet boundary condition, as shown in the Eq.(7): the pouring behaviour is stopped at $t_s$= 10 s. $t_s$= 9.95 s and $t_s$= 10.36 s denote the moments just before and after the pouring stops, respectively. For Fig.6(a), the flow vector direction is pointing towards the risers, indicating that the flow is entering both risers. However, once the pouring behaviour is stopped, a back flow is clearly observed, as shown in Fig.6(b) . This back flow behaviour further results in the decrease of the alloy height in both risers, as shown in Fig.7. Here, $h_1$ (*resp.* $h_3$) and $h_2$ (*resp.* $h_4$) denote the height

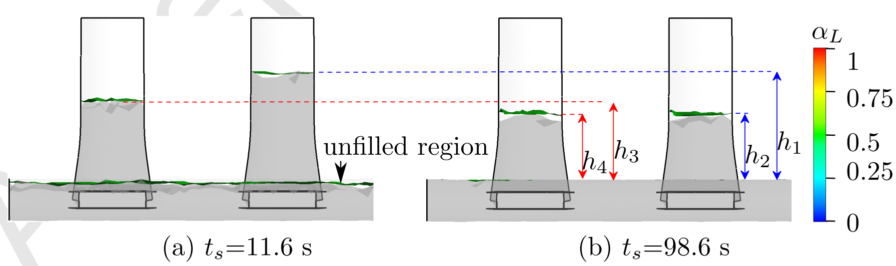


Figure 7: Distributions of the iso-volume of $\alpha_L > 0.5$ (in grey) and iso-surface $\alpha_L = 0.5$ (in green) at different $t_s$. The liquid alloy levels in the risers are decreased and the unfilled volume is refilled at $t_s$=98.6 s compared to $t_s$=11.6 s.

of liquid free level in the front (*resp.* rear) riser at $t_s$= 11.6 s and $t_s$= 98.6 s, respectively. The result clearly showed that the decrease of free level height in the riser as $t_s$ is increased. Meanwhile, the unfilled volume in the runner bar is filled due to this back flow mechanism. The presence of the hole in the front riser, as shown in Fig.1, could be generated through this back flow feature and the shrinkage behaviour.

### *3.3. Mould configuration modification*

The filling simulation for the original sand mould design has revealed the back flow mechanism to shape the runner bar top region. This back flow mechanism requires a certain height of alloy in the risers, which results in the extra alloy wastage. Therefore, an modified configuration mould design was suggested, aiming at eliminate the back flow mechanism so that to reduce the wastage. The modified mould configuration is contrasted to the original design in Fig.8. The

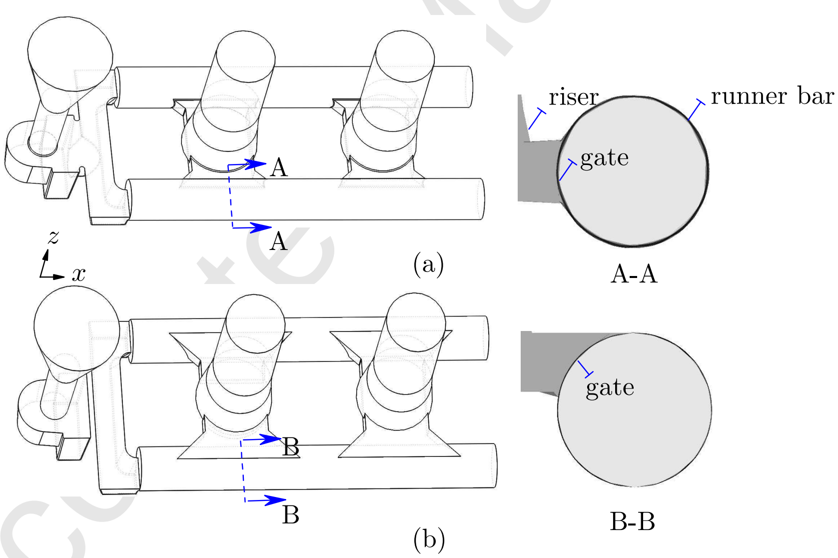


Figure 8: Sketch of the original (a) and improved (b) configuration. The gates for both risers (blue dashed line region) move towards the direction of outlets of the risers.

main difference between the original and the modified configuration is that the location of the gates (from runner bar to riser) for both risers have been lifted upwards (along $z$-axis to the top of the runner bar).

Simulation on the modified configuration is performed under the identical numerical setup conditions of the original design. The filling behaviour of the liquid alloy in Region I is similar with the original configuration. However, different flow behaviour was observed in Region II. Fig.9 showed the snapshots of the interface distribution between the liquid alloy and the air phase at $\alpha_L$=0.5 (in green) for iso-surface and at $\alpha_L > 0.5$ (in grey) for iso-volume at different $t_s$, respectively. The results indicate that after the liquid alloy enters the runner

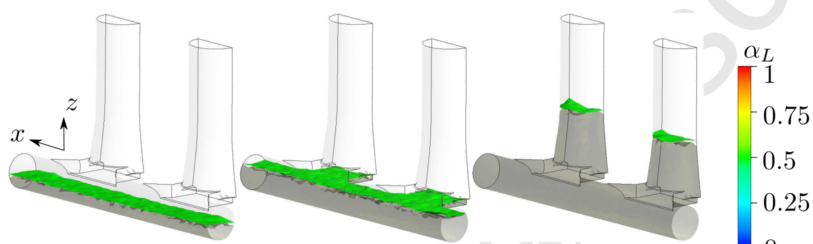


(a) $t_s$=4.75 s (b) $t_s$=7.06 s (c) $t_s$=11.3 s

Figure 9: Snapshots of the iso-volume of $\alpha_L > 0.5$ (in grey) and the iso-surface (in green) at $\alpha_L = 0.5$ distribution for different $t_s$ in Region II for the improved mould design.

bar, the free liquid level increases as the $t_s$ increases, as shown in Fig.9(a). Due to the feature of the improved geometry, which the gates of the risers are located in the vicinity of the top of the runner, the flow enters the risers and the runner bar region simultaneously Fig.9(b). As $t_s$ increases, the runner bar region is filled completely, without the unfilled region Fig.9(c). Compared to the original mould configuration, the essential filling time to shape the cast is reduced to 8.9 s from 10 s. Therefore, for a fixed inlet alloy pouring rate, the amount of the alloy is reduced by around 11%. The improved configuration successfully avoids the existence of the unfilled zone in the runner bar region. This will result in an uniform solidification process and improve the microstructure of the cast.

## 4. Conclusions

This research aimed at figuring out the possible reasons for the alloy wastage in the risers of company supplied mould and eliminating this wastage by optimising the mould design. The main findings were summarized as follows:

- For the original (company supplied) mould design, the results revealed that the main reason for the alloy wastage was due to the existence of the unfilled volume in the vicinity of the runner bar top region. This could be understood as follows. The unfilled volume was refilled by the back flow originated from the risers once the filling was stopped and the back flow dynamics was triggered by a certain height of the alloy in the risers. This certain height of alloy (in the risers) contributed both to refill the unfilled volume and to result in the wastage. Obviously, the wastage should be avoided.

- The modified mould design was obtained by varying the gates (between the runner bar and the riser) location, however, remaining the other part features. The modification was expected to be conducted in small scale therefore to minimize the effect the production process. The results showed that the runner bar unfilled volume was disappeared. The alloy wastage were reduced by 11%.

- This research further indicated that the gates location was an important parameter need to be considered in detail during the mould design.

**Acknowledgements**

The authors would like to acknowledge ASTUTE2020 (Advanced Sustainable Manufacturing Technologies). The Operation has been part-funded by the European Regional Development Fund (ERDF) through the Welsh Government and the participating Higher Education Institutes. Additionally, the authors would like to thank Professor Johann Sienz for his helpful discussion and financial support. Furthermore, the authors would also like to thank the reviewers for their work which has contributed to this paper.

## References

Chan K.S., Pericleous K., Cross M., 1991. Numerical simulation of flows encountered during mold-filling. Appl.Math.Modelling. 15, 625-631.

Ravindran K., Lewis R.W., 1998. Finite element modelling of solidification effects in mould filling. Finite Elements in Analysis and Design. 31, 99-116.

Kim K.D., Yang D.Y., Jeong J.H., 2006. Adaptive refinement techniques based on tetrahedral and hexahedral grids for finite element analysis of mold filling in casting processes. Comput.Methods Appl. Mech. Engrg.. 195, pp 6799-6281.

Pang S., Chen L., Zhang M., Yin Y., Chen T., Zhou J., Liao D., 2010. Numerical simulation two phase flows of casting filling process using SOLA partical level set method. Appl.Math.Modelling.. 34, 4106-4122.

Sirrell B., Holliday M., Campbell J., 1995. The benchmark test 1995. Proceedings of the 7th Conference on Modeling of Casting Welding and Solidification Processes. 915933.

Mirbagheri S.M., Esmaeileian H., Serajzadeh S., Varahram N., Davami P., 2003. Simulation of melt flow in coated mould cavity in the casting process. Journal of Materials Processing Technology. 142, 495-507.

Kermanpur A., Mahmoudi S., Hajipour A., 2008. Numerical simulation of metal flow and solidification in the mult-cavity casting moulds of automotive components. Journal of Materials Processing Technology, 206, 62-68.

Sun Z., Hu H., Chen X., 2008. Numerical optimization of gating system parameters for a magnesium alloy casting with multiple performance characteristics. Journal of Materials Processing Technology. 199, 256-264.

Du J., Chong X., Jiang Y., Feng J., 2015. Numerical simulation of mold filling process for high chromium cast iron matrix composite reinforced by ZTA ceramic particles. International Journal of Heat and Mass Transfer. 89, 872-833.

Assar A.M., 1999. The structure and soundness of Al-4.5Cu ingots cast in open mould using different filling rate. Journal of Materials Processing Technology. 86, 146-151.

Cox M., Wickins M., Kuang J.P., Harding R.A., Campbell J., 2000. Effect of top and bottom filling on reliability of investment castings in Al, Fe, and Ni based alloys. Materials Science and Technology. 16, 1445-1452.

Carswell D., Davies M.H., Lavery P.N., James J., Brown G.R.S., Fourlaris G., 2011. Simulation for mould design of a gravity sand casting (final report). Unpublished internal report. ASTUTE Project Office contact: Tel. +44 1792 606378, Email: info@astutewales.com.

Sun D., Xu J., Wang L., 2012. Development of a vaporliquid phase change model for volume-of-fluid method in FLUENT. International Communications in Heat and Mass Transfer. 39(8), 1101-1106.

Hargreaves D.M., Morvan H.P., Wright N.g., 2014. Validation of the volume of fluid method for free surface calculation: the broad-crested weir. Engineering Applications of Computational Fluid Mechanics. 19(2), 136-146.

ANSYS Fluent User's Guide V15.0., 2013.

Joel H. Ferziger, Milovan Peric, 2002. Computational Methods for Fluid Dynamics; third, rev. edition. Springer-Verlag Berlin Heidelberg New York.

Hunt J.C.R., Abell C.J., Peterka J.A., Woo H., 1978. Kinematical studies of the flows around free o surface-mounted obstacles; applying topology to flow visualization. J.Fluid Mech.. 86(1), 179-200.

Zhang L., Potherat A., 2013. Influence of the geometry on the two- and three-dimensional dynamics of the flow in a 180$^o$ sharp bend. Physics of Fluids. 25, 053605.

Jolly M., 2005. Prof. John Campbell's ten rules for making reliable castings. JOM May, 19-28.

Campbell J., 2004. Casting Practice The 10 Rules of Castings; Elsevier Butterworth-Heinemann Linacre House, Jordan Hill, Oxford, UK, OX2 8DP.